Research Article

Journal of MASS SPECTROMETRY

Received: 11 January 2010 Accepted: 8 March 2010 Published online in Wiley Interscience: 29 March 2010

(www.interscience.com) DOI 10.1002/jms.1739

An experimental and computational study on the dissociation behavior of hydroxypyridine *N*-oxides in atmospheric pressure ionization mass spectrometry

Matias Butler,[a] Pau Arroyo Mañez[b] and Gabriela M. Cabrera[a]*

A tandem mass spectrometric study of protonated isomeric hydroxypyridine *N*-oxides was carried out with a hybrid quadrupole/time-of-flight mass spectrometer coupled with different atmospheric pressure ionization sources. The behavior observed in the collision-induced dissociation (CID) mass spectra of the parent cations, was similar irrespective of the source employed. However, there were intrinsic differences in the intensities of the two fragments observed for each isomer. The major fragment because of elimination of a hydroxyl radical, dominated the CID spectra (in contrast with weaker water loss) at different energy thresholds. Therefore, it was possible to differentiate both isomers at collision energies above 13 eV by comparing the ratio of intensities of the major fragment relative to the precursor cation. In addition, quantum chemical calculations at the B3LYP/6-31++G(d,p) level of theory were performed for the protonated isomers of hydroxypyridine *N*-oxide and their radical cation products in order to gain insight into the major routes of dissociation. The results suggest that dissociation from the lowest triplet excited state of the protonated species would provide a reasonable rationalization for the difference in behavior of both isomers.

Supporting information may be found in the online version of this article.

Keywords: pyridine *N*-oxides; CID fragmentation; isomer differentiation; API MS; *ab initio* calculations

Introduction

Pharmaceuticals and their metabolites have become an increasing public concern as their potential impacts on the environment are revealed.[1] In particular, pyridine and its derivatives are of immense relevance because they are known for their toxic and carcinogenic properties and their lethal effects on the natural biogenic environment.[2] Heterocyclic *N*-oxides are present in pharmaceuticals, agrochemicals and synthetic intermediates,[3] but they are also common metabolites that can be formed by *N*-atom oxidation during metabolic biotransformation, an important pathway for many drugs and xenobiotics.[4]

Differentiation by mass spectrometry of heterocyclic *N*-oxides and their isomeric hydroxylated metabolites is of interest because their product ion spectra are usually very similar, particularly when *N*-oxidation or hydroxylation occurs on the same aromatic ring.[5] Therefore, a detailed understanding of the ionization and fragmentation of heterocyclic *N*-oxides would be very valuable.[6] While the hydroxypyridines have been extensively studied by mass spectrometry,[7,8] to our knowledge their *N*-oxides have thus far escaped examination.

In the present work, a hybrid quadrupole/time-of-flight (QTOF) mass spectrometer with electrospray ionization (ESI), At-mospheric Pressure Chemical Ionization (APCI) and Atmospheric Pressure PhotoIonization (APPI) sources, was employed to study the tandem mass spectrometric (MS/MS) behavior of 2-hydroxypyridine *N*-oxide **1** and 3-hydroxypyridine *N*-oxide **2** (Fig. 1). 2-hydroxypyridine *N*-oxide **1** exists as a tautomeric mixture **1-a** and **1-b**, being **1-a** the main tautomer in solution and in the crystal state.[31] In order to achieve a better understanding of the fragmentation mechanism, *ab initio* computational calculations were also performed. Characterization of the main ions obtained and analysis of the relative stability of the possible isomers and their primary dissociation products may provide an important tool to distinguish the fragmentation pattern of both hydroxypyridine *N*-oxide isomers. Provided a sufficiently accurate level of approximation is available, the details of the potential energy surface (PES) may give rise to a consistent picture of the course of events leading to the observed reaction. Furthermore, the type of insight available from the model may not be easily available through the experiment and it may, therefore, be unique.[9]

* *Correspondence to: Gabriela M. Cabrera, Departamento de Química Orgánica, UMYMFOR-CONICET, Facultad de Ciencias Exactas y Naturales, Universidad de Buenos Aires. Ciudad Universitaria, Buenos Aires, Argentina. E-mail: gabyc@qo.fcen.uba.ar*

a *Departamento de Química Orgánica, UMYMFOR-CONICET, Facultad de Ciencias Exactas y Naturales, Universidad de Buenos Aires. Ciudad Universitaria, Buenos Aires, Argentina*

b *Departamento de Química Inorgánica, Analítica, y Química Fisica, INQUIMAE-CONICET, Facultad de Ciencias Exactas y Naturales, Universidad de Buenos Aires. Ciudad Universitaria, Buenos Aires, Argentina*

Journal of MASS SPECTROMETRY

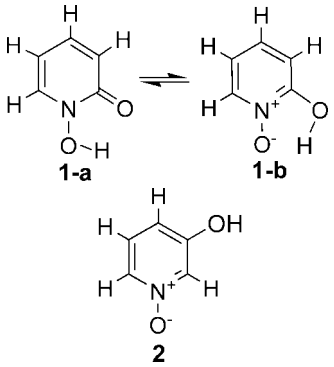

Figure 1. Structures of the *N*-oxides studied.

Table 1. Typical API sources operational parameters

Parameter	Setting		
	ESI	APCI	APPI
End plate offset (V)	−500	−500	−500
Cappilary (kV)	4.5	4	4.2
Nebulizer (bar)	0.4	2.0	2.0
Dry gas (N_2) (l min^{-1})	4.0	3.0	3.0
Dry temperature (°C)	180	180	180
Vaporizer temperature (°C)	NA	180	180
Photoenergy of Krypton discharge lamp (eV)	NA	NA	10
Corona (mA)	NA	4000	NA

Experimental and Theoretical Methods

Materials

2-hydroxypyridine *N*-oxide and 3-hydroxypyridine *N*-oxide were purchased from Sigma-Aldrich (Milwaukee, WI, USA). LCMS grade methanol and HPLC grade water were purchased from Carlo Erba. Ammonium acetate, puriss. p.a. for MS, was purchased from Sigma-Aldrich. The analyte solutions, each at a concentration of 1 mg ml^{-1}, were prepared using methanol. In the case of ESI, 50 µl of an ammonium acetate 10 mM solution in methanol and water (50 : 50) were added to solutions of each compound prior to infusion into the mass spectrometer.

Mass spectrometry

Mass spectrometric analyses were performed using a Bruker micrOTOF-Q II mass spectrometer (Bruker Daltonics, Billerica, MA, USA), equipped with ESI, APCI or APPI sources. Typical operating conditions of API sources are summarized in Table 1.

The quadrupole mass filter was set normally with a 1.0 Da window for transmission (isolation) of precursor ions. Fragmentation of the mass-selected ions (collision-induced dissociation; CID) was performed in a radiofrequency-only quadrupole collision cell with ultra high purity (UHP) Argon as collision gas. Multi-point mass calibration was carried out using a mixture of sodium formate from *m/z* 50 to 900 in positive-ion mode. Data acquisition and processing were carried out using the Bruker Compass Data Analysis version 4.0 software supplied with the instrument.

Solutions of *N*-oxides were infused into the sources using a KDS 100 syringe pump (KD Scientific, Holliston, MA, USA) at a flow rate of 180 µl min^{-1}.

Each experiment was repeated at least three times in different days in order to ensure reproducibility.

Computational calculations

All calculations were performed using the Gaussian 03 computational package.[10] Geometries of neutral and protonated molecules, as well as transition structures and products were optimized at the B3LYP hybrid density functional level of theory (DFT)[11,12] using the 6-31++G(d,p) basis set. This basis set featuring both polarized and diffuse orbitals on each atom proved to be well suited for investigating systems with delocalized charges.[13]

The most probable sites of protonation for the neutral molecules were determined through analysis of the electrophilic Fukui function,[14] as well as comparing the relative energies between the possible protonated species.

The optimized structures were characterized by harmonic frequency analysis as local minima (all frequencies real) or first order saddle points (one imaginary frequency). Intrinsic reaction coordinate (IRC) calculations[15] were also performed in order to verify that localized transition state structures were connected with the corresponding minimum stationary points associated with reactants and products.

Spin unrestricted calculations (UB3LYP) were used for open-shell systems. Furthermore, in order to confirm that the relative energies obtained draw the correct trend, single-point restricted open-shell (ROMP2) calculations[16] were carried out for the entire set of previously optimized structures to deal with spin contamination.[17]

Calculations were performed in the Centro de Cómputos de Alto Rendimiento, Facultad de Ciencias Exactas y Naturales, Universidad de Buenos Aires.

Results and Discussion

Dissociation characteristics

CID behavior

Protonated cations of **1** and **2** were readily produced, in the gas phase, from the corresponding neutral molecules, using ESI, APCI or APPI. The conditions employed for the experiments are described in Table 1 and the aim was to keep the mutual parameters as similar as possible in order to ascertain the effect of the different sources.

The ESI CID mass spectra of the protonated cations of the two isomeric ions at 15 eV are presented in Fig. 2. It is readily seen from Fig. 2 that these spectra are distinctly different. They exhibit only two product ions, one even mass and one odd mass ion, which correspond to the loss of a neutral and the loss of a radical, respectively. Significant differences in the dissociation behavior for other collision energies are also observed, as shown in Fig. 3. The signal at *m/z* 95 (loss of HO•) dominates the product ion spectrum of the protonated precursor of **2** at collision energies above 13 eV, whereas loss of water is negligible. On the other hand, the parent protonated cation of **1** dominates the spectrum at all collision energies; the loss of the radical and water are comparable until 10 eV, when the radical loss becomes slightly more important (Fig. 4).

Although the CID behavior is contrary to the 'even electron rule', there are documented exceptions to this empirical prediction that seem not to be valid for compounds whose fragment ions conserve

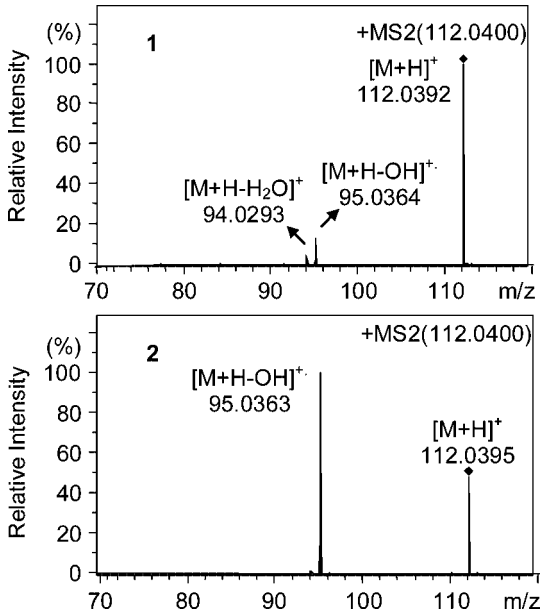

Figure 2. CID spectra recorded for electrospray produced protonated hydroxypyridine *N*-oxides. ESI-MS/MS spectrum of protonated **1** or **2** precursor at *m/z* 112 with collision energy of 15 eV.

a strong ability to stabilize unpaired electrons.[18] In these cases, the formation of two open-shell species by CID of a precursor may be more favored than the loss of a closed shell neutral and the formation of a product cation.[19]

The product ion spectra obtained with ESI were closely similar to the CID spectra obtained with APCI and APPI, as displayed in Fig. 4, except for the absolute intensities which differ according to the sensitivity of each method. ESI and APCI showed comparable intensities, the latter being slightly superior, whereas APPI exhibited about half the absolute values of the other sources.

In conclusion, it was possible to easily differentiate both isomers at collision energies above 13 eV by comparing the ratio of intensities of the precursor and the *m/z* 95 fragment. A ratio $[M+H]^+/[M+H-OH]^+$ higher than 1, is exclusive for **1**.

Effect of temperature

The effect of temperature on the dissociation behavior of isomeric *N*-oxide precursor ions was studied with the APCI source varying the vaporizer temperature from 180 to 400 °C. Maximum sensibility in ion abundance was found for both compounds between 200 and 225 °C. In the mass spectra of both compounds the enhancement in the intensity of the *m/z* 96 ion because of loss of oxygen at temperatures above 300 °C were observed, as shown in Fig. 5. An associated increase in deoxygenation with temperature elevation was consistently observed although the extent differed between the two compounds. These findings are in agreement with those reported earlier for quinoline *N*-oxide derivatives and other compounds with the *N*-oxide moiety.[5,6,20] Complete lack of formation of the deoxygenated fragment ions in APCI MS/MS and formation in APCI MS led to the above-mentioned authors suggesting that the fragmentation of *N*-oxides leading to deoxygenation is because of thermal activation and not induced by collisional activation.

Tandem mass spectra of the protonated cations of **1** and **2** were registered at different temperatures and the results showed no significant temperature dependence. No substantial changes were observed, which suggest that thermal activation is not an important factor in the actual dissociations.

Reaction mechanism studies

Protonation sites

The first step in the mass spectrum interpretation of ionized substances by protonation is the determination of the site in which this process occurs.[21] In this context, local reactivity indices such as the atomic nucleophilic indices (f_k^-) also known as electrophilic Fukui functions provide an interesting alternative way to identify the most probable sites of protonation.[14] Recently, this methodology has been employed to identify the protonation sites in a series of natural and synthetic compounds.[22,23]

In order to estimate the condensed Fukui function, three approaches were employed: the finite-difference approximation[24], using Mulliken population analysis (MPA)[25] and natural population analysis (NPA)[26] charges, as well as the frontier molecular orbitals direct approach, related to the electronic density and

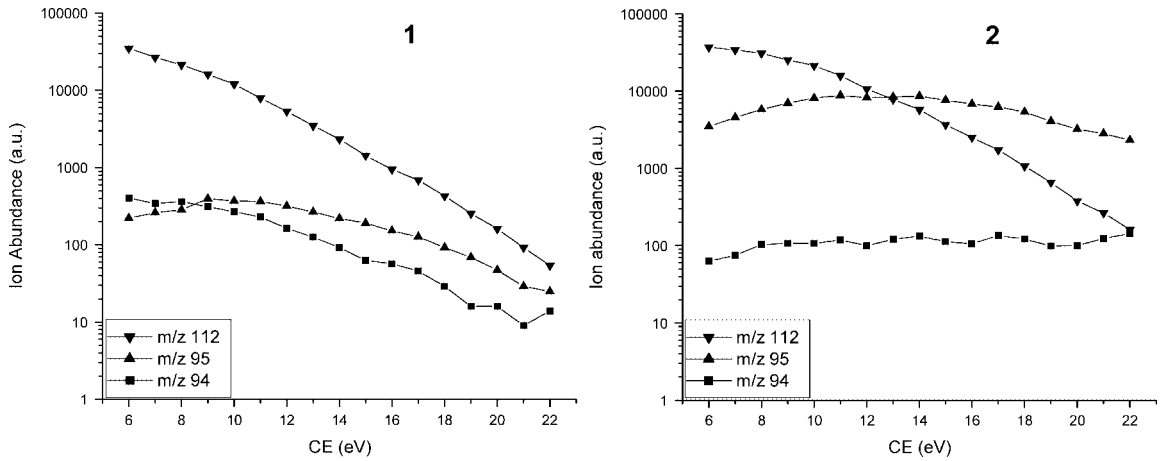

Figure 3. Breakdown diagrams showing ion abundance (arbitrary units) versus collision energy (eV) for MS/MS of protonated hydroxypyridine *N*-oxides ions obtained from electrospray experiments. The plots show the evolution of protonated **1** or **2**, and fragment ions representing two competing pathways (*m/z* 112 = protonated precursor; *m/z* 95 = $[M+H-OH]^{+\bullet}$; *m/z* 94 = $[M+H-H_2O]^+$).

Journal of MASS SPECTROMETRY

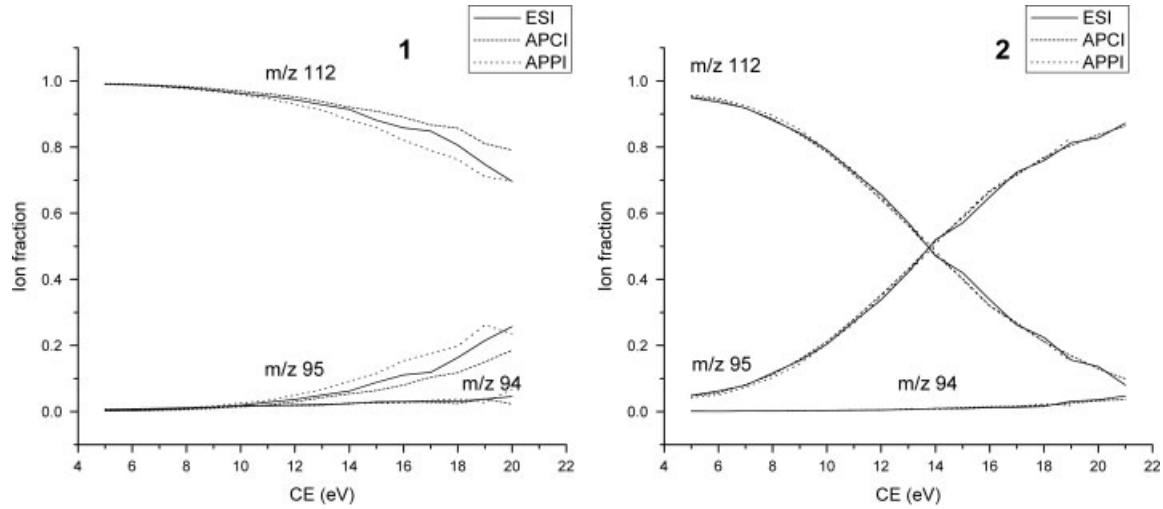

Figure 4. Breakdown diagrams showing fractional abundance versus collision energy (eV) for MS/MS of protonated hydroxypyridine *N*-oxides ions obtained from ESI, APCI and APPI experiments. The plots show the evolution of protonated **1** or **2**, and fragment ions representing two competing pathways (*m/z* 112 = protonated precursor; *m/z* 95 = $[M+H-OH]^+$; *m/z* 94 = $[M+H-H_2O]^+$).

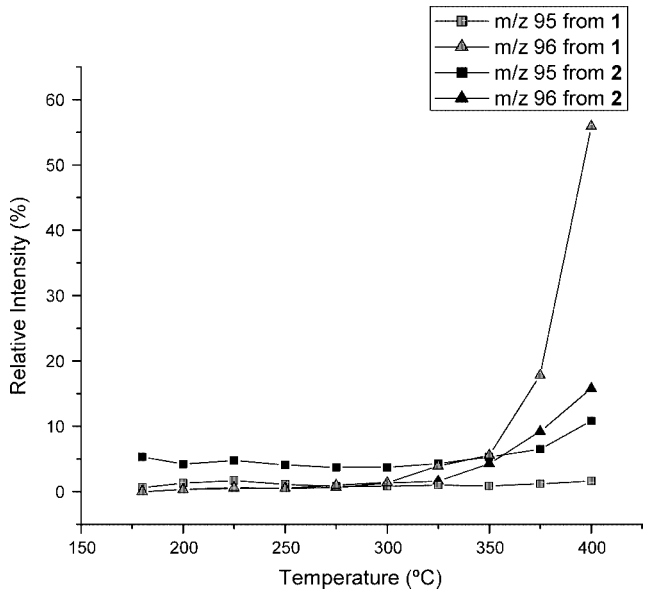

Figure 5. Ratio of the ion intensity of dehydroxylated (*m/z* 95) and deoxygenated (*m/z* 96) products relative to the parent protonated **1** and **2** at different vaporizer temperatures in the APCI mass spectra of hydroxypyridine *N*-oxides.

localization of the HOMO in the molecule, neglecting the overlap term.[27]

The probable protonation sites obtained by the calculations depicted above are summarized in Table 2. These values show that the oxygen atom of the *N*-oxide moiety in **1-b** and **2,** and the carbonyl oxygen in **1-a** are the preferred sites. Later, precursor cations were produced by protonation of **1-a, 1-b** as well as **2** and the protonation energies of all possible cations were calculated (Table 3). Relative energies confirm the results obtained by the local electrophilic Fukui indices.

Protonation of **1-a** (−217.6 kcal mol^{-1}) and **1-b** (−219.8 kcal mol^{-1}) according to the most favored positions (Table 3) led to the same product ion. In each case, one stable conformation was found from **1-a** and **1-b** and named **I** + **H** and **II** + **H**, respectively. Two stable conformations were also found upon protonation of **2** (−225.7 kcal mol^{-1}), **III** + **Ha** and **III** + **Hb** (Fig. 6), but given the similar results obtained with both (relative energy differences between respective structures minor to 1 kcal mol^{-1} in all succeeding cases), any of them resulted equally representative and was subsequently named **III** + **H** (vide infra).

Protonation at the already protonated oxygen of the *N*-oxide moiety in **1-a** and at the oxygen of the hydroxyl group in **1-b** resulted in the respective geometry optimizations in unstable ions which rearranged to the most stable ions **II** + **H** and **I** + **H**, respectively. Similarly, protonation at N-1, C-3 and C-5 in **1-b** did not result in stable ions; instead, upon attempted geometry optimizations the structures rearranged, through proton migration from the OH group onto the oxygen of the *N*-oxide moiety, to the respective structures found for **1-a.**

Ion energetics

A better characterization of the relevant ionic structures in the dissociation of the cations **I** + **H**, **II** + **H** and **III** + **H**, was carried out by exploratory *ab initio* calculations. A full geometry optimization was performed for the reactant and primary product ions of the major dissociation reactions, obtaining the most stable conformations of the protonated hydroxypyridine *N*-oxide isomers and the respective products. The most relevant optimum geometrical parameters of the protonated cations obtained from the calculations are displayed in Fig. 6. Frequency analysis of the stationary structures obtained was performed to complete the characterization.

As seen in Fig. 6, the hydroxyl group substituent is found to be coplanar with the aromatic ring in the most stable conformations of all the studied isomers. This result shows the greater effectiveness of the interaction of the π lone electronic pair of the oxygen atom with the aromatic ring π orbitals relative to the corresponding interaction involving the σ lone electronic pair. On the other hand, the protonated oxygen group of the *N*-oxide moiety is found to be oriented almost perpendicular to the aromatic ring, except for **I** + **H** where the group is found to be coplanar. In both conformations of the 2-substituted isomers, the hydroxyl groups are oriented *cis* relative to each other, a fact which

Table 2. Condensed Fukui functions for electrophilic attack for the isomeric hydroxypyridine N-oxides

Method	MPA f_k^-			NPA f_k^-			HOMO f_k^-		
Site (k)	1-a	1-b	2	1-a	1-b	2	1-a	1-b	2
N-1	0.05	−0.01	−0.01	0.08	−0.02	−0.05	0.19	0.10	0.04
C-2	−0.04	0.01	0.03	−0.02	0.08	0.07	0.03	0.11	0.07
C-3	0.16	0.07	0.00	0.15	0.02	0.01	0.15	0.01	0.02
C-4	−0.02	0.08	0.19	0.00	0.13	0.20	0.00	0.10	0.19
C-5	0.16	0.07	0.00	0.19	0.07	−0.01	0.20	0.06	0.01
C-6	0.02	0.01	0.07	0.05	0.04	0.13	0.06	0.03	0.14
N–O	0.12	**0.37**	**0.37**	0.11	**0.40**	**0.40**	0.09	**0.51**	**0.51**
C–O	**0.25**	0.12	0.07	**0.27**	0.11	0.06	**0.29**	0.09	0.02

Values in bold indicate the preferred site of protonation for each isomer.

Table 3. Protonation energies (kcal mol^{-1}) for the isomeric hydroxypyridine *N*-oxides

	1-hydroxypyridine-2-one 1-a		2-hydroxypyridine *N*-oxide 1-b		3-hydroxypyridine *N*-oxide 2	
Position	dE	dE rel	dE	dE rel	dE	dE rel
N-1	−177.6	39.96	[a]	[a]	−176.9	48.79
C-2	−167.6	50.01	−172.5	47.36	−197.7	28.01
C-3	−198.7	18.86	[a]	[a]	−153.5	72.20
C-4	−164.9	52.69	−183.2	36.63	−199.9	25.83
C-5	−198.5	19.08	[a]	[a]	−166.9	58.80
C-6	−170.9	46.70	−183.8	36.07	−201.1	24.63
N–O	[a]	[a]	**−219.8**	**0**	**−225.7**	**0**
C–O	**−217.6**	**0**	[a]	[a]	−171.3	54.34

dE, energy difference between the neutral and protonated molecule; dE rel, energy difference relative to the most stable protonated isomer.
[a] Unstable ions. Values in bold indicate the most favored site of protonation for each isomer.

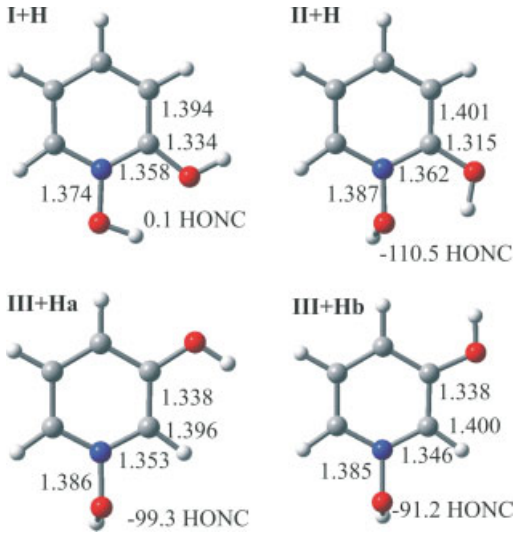

Figure 6. UB3LYP/6-31++G(d,p) optimized geometries of the protonated cations of **1** and **2**, showing C2–C3, N1–C2, C–O and N–O bond distances in angstroms and dihedral angles H–O1–N1–C2 in degrees. (The dissociation products and interconnecting structures are available in the Supporting information).

possibly facilitates the occurrence of further stabilizing interactions (hydrogen bonds) between them.

The energy profiles for the protonated hydroxypyridine *N*-oxide isomers and their interconnecting structures and primary dissociation products are presented in Fig. 7. For the sake of simplicity in the presentation of data, the calculated total and zero point energies are omitted. A comparison between the two sets of energy data suggests that the ROMP2//UB3LYP/6-31++G(d,p) energy differences between the various ions, diagrammatically shown in Fig. 7, are in all cases higher by a few kilocalories per mole than those formerly obtained with UB3LYP/6-31++G(d,p). Taking into account both sets of energy data, it can be concluded that the hydroxyl group is lost preferentially from the *N*-oxide moiety and not from the aromatic ring. For this reason, in the following section this pathway is the one considered.

Dissociation pathways

The dissociation pathways of **I** + **H**, **II** + **H** and **III** + **H** cations were studied by localization of the transition structures which were characterized by the imaginary frequency calculation. Unfortunately, all attempts to locate a transition structure for hydroxyl radical loss from protonated reactants for the ground electronic state (singlet) failed. Furthermore, the PES scan for **I** + **H**, **II** + **H** and **III** + **H** showed no transient structure accounting for the radical loss. Sometimes the formation of radicals may occur with the involvement of an electronically excited state such as the triplet state.[28]

Taking into account the afore-mentioned, the dissociation pathways of **I** + **H**, **II** + **H** and **III** + **H** cations in the excited triplet state were studied similarly. Hence, it was possible to characterize the triplet PES which comprised a transition structure for hydroxyl radical loss from protonated reactants **I** + **H** and **III** + **H**; but not

Journal of MASS SPECTROMETRY

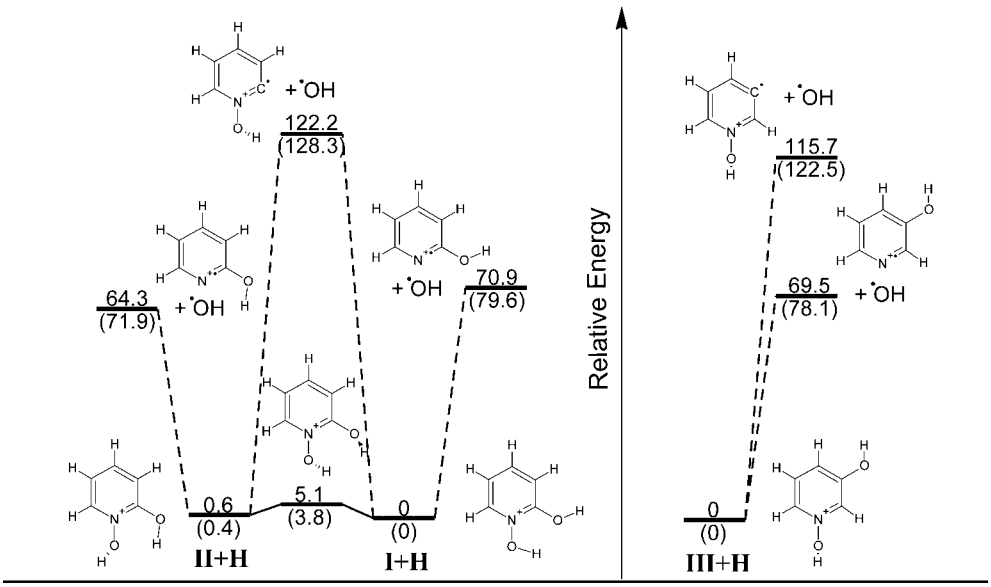

Figure 7. Energy profiles for the protonated hydroxypyridine *N*-oxide isomers and their interconnecting structures and primary dissociation products. All values are in kcal mol^{-1}. The energies are from UB3LYP/6-31++G(d,p) calculations. Values in parentheses are from ROMP2//UB3LYP/6-31++G(d,p) energy calculations.

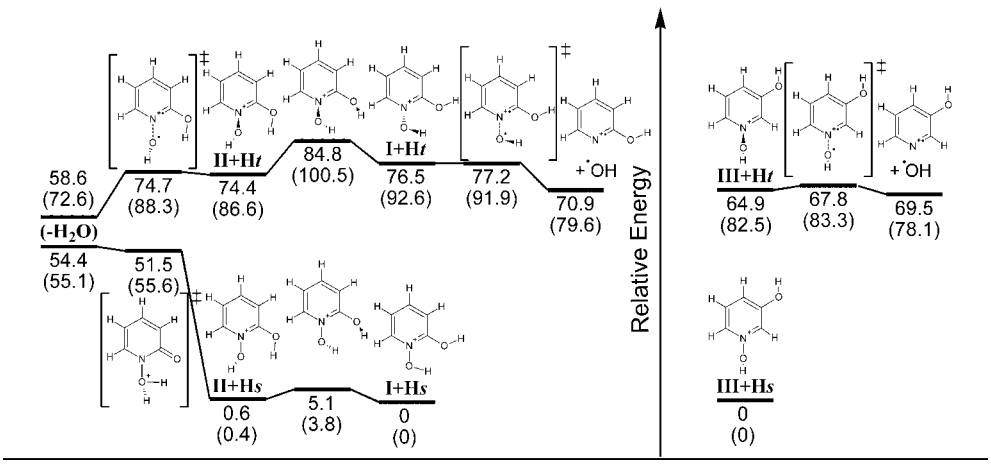

Figure 8. Potential energy profile for the protonated hydroxypyridine *N*-oxide isomers along with their major dissociation pathways. All values are in kcal mol^{-1}. The energies are from UB3LYP/6-31++G(d,p) calculations. Values in parentheses are from ROMP2//UB3LYP/6-31++G(d,p) energy calculations. The structures signaled by ***s*** correspond to the initial structures (parent ions) of the singlet protonated compounds, whereas the structures signaled by ***t*** correspond to the initial structures (parent ions) of the triplet protonated compounds.

for **II** + **H** whose transient structure was responsible for water loss as confirmed by IRC calculations. This loss was also found serendipitously while searching hydroxyl radical loss in **II** + **H** in the ground state (vide infra).

The potential energy profiles for the protonated hydroxypyridine *N*-oxide isomers along their major dissociation pathways are presented in Fig. 8. The most relevant geometrical parameters of the optimized structures dealing with the dissociation pathways of **I** + **H**, **II** + **H** and **III** + **H** are depicted in Fig. 9. When comparing the protonated reactants in the singlet and triplet states, it can be seen that the N–O bond length is longer in the latter and the bond is no longer coplanar with the aromatic ring, presenting a deformation in the dihedral angle O–N1–C2–C3. Regarding the transition state structures, it can be seen that they resemble the triplet parent cations but with a much longer N–O length.

The relative differences between UB3LYP and ROMP2 values amount to, at most, 18 kcal mol^{-1}, and are thus quite acceptable for our present qualitative purpose. Nevertheless, both methods are consistent in predicting a higher barrier for the hydroxyl loss in **I** + **H** with respect to **III** + **H**, by about 10 kcal mol^{-1}. This energetic barrier difference might be responsible for the different relative intensities of the fragments observed previously in the mass spectra of each compound for a given collision energy (Figs 2 and 3).

The PESs of **I** + **H** and **III** + **H** cations were explored by stepwise increasing the length of the breaking bond (N–O) and the dihedral angle O–N1–C2–C3, while optimizing all other coordinates at each given bond length and dihedral angle (Fig. 10). Along with the N–O bond elongation, the calculated PES scan of the singlet ground state and the triplet excited state cross at a certain point which corresponds to an N–O bond length of approximately

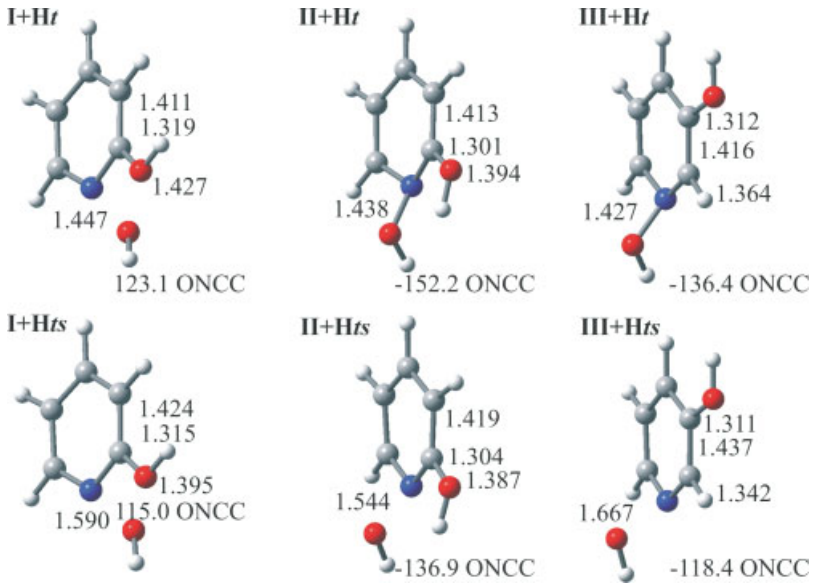

Figure 9. UB3LYP/6-31++G(d,p) optimized geometries of the protonated cations of **1** and **2** in the triplet state ***t*** and transition structures ***ts*** showing C2–C3, N1–C2, C–O and N–O bond distances in angstroms and dihedral angles O1-N1-C2-C3 in degrees. (The dissociation products and interconnecting structures in the triplet state are available in the Supporting information).

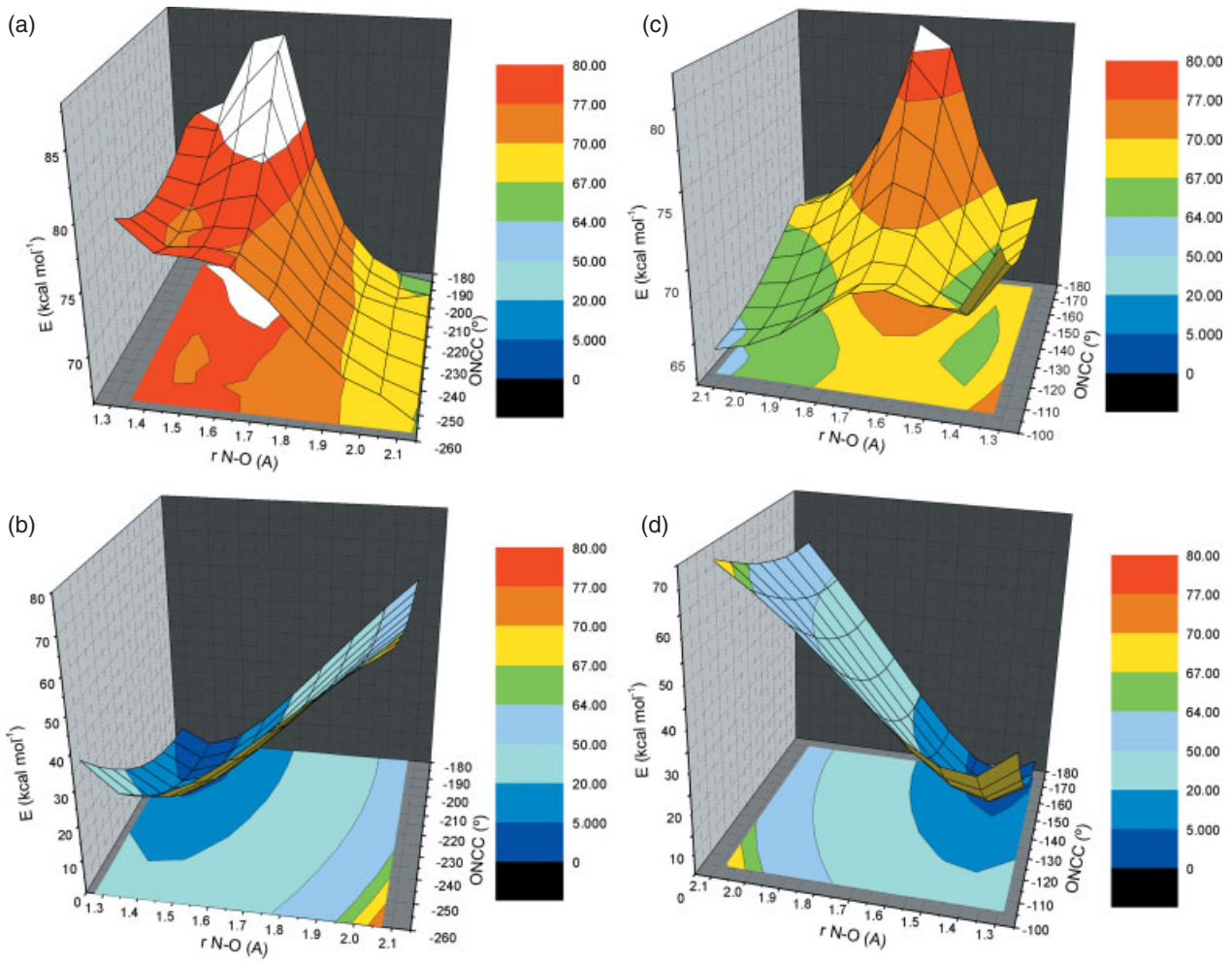

Figure 10. PES exploration by UB3LYP/6-31++G(d,p) for the protonated compounds: **I** + **H** (panels a and b); and **III** + **H** (panels c and d), comprising the triplet excited (panels a and c) and singlet ground (panels b and d) electronic states.

2.0 Å. Nonetheless, the energy values at these crossing points are very similar as they are close to the respective products and thus, this mechanism provides no justification for the differences observed between both isomers. On the other hand, the vertical singlet-triplet transition, although more endoergic, reproduces the energetic barrier differences found previously.

The use of the DFT method allowed us to avoid the problem of spin contamination observed in UHF (MP2) wave functions, which could be severe and is certainly found in some doublet and triplet states.[29] All spin expectation values $<S^2>$ of the open-shell systems were within 2% of the expected value and showed that the B3LYP wave functions do not suffer appreciably from spin contamination.

The mechanism presented above is not exclusive albeit it is consistent with the experimental data available. There is evidence for the involvement of the triplet state in the deoxygenation of heteroaromatic *N*-oxides,[30] hence the results obtained support the suggestion that the hydroxyl radical dissociation mechanism occurs, assuming fragmentation from the lowest triplet excited state.

Conclusions

The dissociation behavior in positive-ion mode atmospheric pressure mass spectrometry of two representative hydroxypyridine *N*-oxides, via CID in a QTOF mass spectrometer, was investigated. Two competing fragmentation pathways were the loss of either a hydroxyl radical or water and, in contrast with the even electron rule, the CID spectra were dominated by the former pathway at different energy thresholds for each isomer. Both isomers could easily be distinguished at collision energies above 13 eV by comparing the ratio of intensities of the precursor and the fragment corresponding to hydroxyl radical loss.

Upon structural optimization of protonated reactant precursors using B3LYP/6-31++G(d,p), it could be concluded that the hydroxyl group is lost preferentially from the N-oxide moiety and not from the aromatic ring. The PES scan for the ground electronic state (singlet) in the protonated molecules showed no transient structure accounting for the radical loss. However, the triplet PES comprised a transition structure for hydroxyl radical loss from protonated reactants, predicting a higher barrier for the hydroxyl loss in one isomer with respect to the other by about 10 kcal mol^{-1}. This energetic barrier difference might be responsible for the different relative intensities of the fragments observed previously in the mass spectra of each compound for a given collision energy. Quantum chemical calculations at the B3LYP/6-31++G(d,p) level of theory suggest that fragmentation from the lowest triplet excited state of the protonated species provide a reasonable rationalization for the difference in dissociation behavior of both isomers.

Acknowledgements

We thank Universidad de Buenos Aires for financial support (X029) and CONICET for the fellowships to M. B. and P. A. M. We thank Centro de Cómputos de Alto Rendimiento (CeCAR) at the Facultad de Ciencias Exactas y Naturales (FCEN) of the Universidad de Buenos Aires.

Supporting information

Supporting information may be found in the online version of this article.

References

[1] S. Kim, D. S. Aga. Potential ecological and human health impacts of antibiotics and antibiotic-resistant bacteria from wastewater treatment plants. *J. Toxicol. Environ. Health B* **2007**, *10*, 559.
[2] K. V. Padoley, S. N. Mudliar, R. A. Pandey. Heterocyclic nitrogenous pollutants in the environment and their treatment options – an overview. *Bioresour. Technol.* **2008**, *99*, 4029.
[3] A. Albini, S. Pietra. *Heterocyclic N-oxides*. CRC Press: Boca Raton, **1991**.
[4] P. Hlavica. Biological oxidation of nitrogen in organic compounds and disposition of *N*-oxidized products. *CRC Crit. Rev. Biochem.* **1982**, *12*, 39.
[5] D. M. Peiris, W. Lam, S. Michael, R. Ramanathan. Distinguishing *N*-oxide and hydroxyl compounds: impact of heated capillary/heated ion transfer tube in inducing atmospheric pressure ionization source decompositions. *J. Mass Spectrom.* **2004**, *39*, 600.
[6] W. Tong, S. K. Chowdhury, J.-C. Chen, R. Zhong, K. B. Alton, J. E. Patrick. Fragmentation of *N*-oxides (deoxygenation) in atmospheric pressure ionization: investigation of the activation process. *Rapid Commun. Mass Spectrom.* **2001**, *15*, 2085.
[7] M. A. Trikoupis, P. Gerbaux, D. J. Lavorato, R. Flammang, J. K. Terlouw. Hydrogen-shift isomers of ionic and neutral hydroxypyridines: a combined experimental and computational investigation. *Int. J. Mass Spectrom.* **2002**, *217*, 1.
[8] J. K. Wolken, F. Turecek. Modeling nucleobase radicals in the gas phase. Experimental and computational study of 2-hydroxypyridinium and 2-(1H)pyridone radicals. *J. Phys. Chem. A* **1999**, *103*, 6268.
[9] E. Uggerud. Theory and experiment in mass spectrometry: a perspective on the relationship between computational modelling and experiment in gas-phase ion chemistry. *Eur. J. Mass Spectrom.* **2007**, *13*, 97.
[10] M. J. Frisch, G. W. Trucks, H. B. Schlegel, G. E. Scuseria, M. A. Robb, J. R. Cheeseman, J. A. Montgomery Jr, T. Vreven, K. N. Kudin, J. C. Burant, J. M. Millam, S. S. Iyengar, J. Tomasi, V. Barone, B. Mennucci, M. Cossi, G. Scalmani, N. Rega, G. A. Petersson, H. Nakatsuji, M. Hada, M. Ehara, K. Toyota, R. Fukuda, J. Hasegawa, M. Ishida, T. Nakajima, Y. Honda, O. Kitao, H. Nakai, M. Klene, X. Li, J. E. Knox, H. P. Hratchian, J. B. Cross, C. Adamo, J. Jaramillo, R. Gomperts, R. E. Stratmann, O. Yazyev, A. J. Austin, R. Cammi, C. Pomelli, J. W. Ochterski, P. Y. Ayala, K. Morokuma, G. A. Voth, P. Salvador, J. J. Dannenberg, V. G. Zakrzewski, S. Dapprich, A. D. Daniels, M. C. Strain, O. Farkas, D. K. Malick, A. D. Rabuck, K. Raghavachari, J. B. Foresman, J. V. Ortiz, Q. Cui, A. G. Baboul, S. Clifford, J. Cioslowski, B. B. Stefanov, G. Liu, A. Liashenko, P. Piskorz, I. Komaromi, R. L. Martin, D. J. Fox, T. Keith, M. A. Al-Laham, C. Y. Peng, A. Nanayakkara, M. Challacombe, P. M. W. Gill, B. Johnson, W. Chen, M. W. Wong, C. Gonzalez, J. A. Pople, *Gaussian 03, Revision C.02*. Gaussian, Inc.: Wallingford CT, **2004**.
[11] C. Lee, W. Yang, R. G. Parr. Development of the Colle-Salvetti correlation-energy formula into a functional of the electron density. *Phys. Rev. B* **1988**, *37*, 785.
[12] A. D. Becke. Density-functional thermochemistry. III. The role of exact Exchange. *J. Chem. Phys.* **1993**, *98*, 5648.
[13] A. M. El-Nahas, K. Hirao. A theoretical study on 2-hydroxypyrazine and 2,3-dihydroxypyrazine: tautomerism, intramolecular hydrogen bond, solvent effects. *J. THEOCHEM* **1999**, *459*, 229.
[14] P. Fuentealba, P. Pérez, R. Contreras. On the condensed Fukui function. *J. Chem. Phys.* **2000**, *113*, 2544.
[15] C. Gonzalez, H. B. Schlegel. An improved algorithm for reaction path following. *J. Chem. Phys.* **1989**, *90*, 2154.
[16] R. McWeeny, G. Diercksen. Self-consistent perturbation theory. II. Extension to open shells. *J. Chem. Phys.* **1968**, *49*, 4852.
[17] C. J. Parkinson, P. M. Mayer, L. Radom. An assessment of theoretical procedures for the calculation of reliable radical stabilization energies. *J. Chem. Soc. Perkin Trans. 2* **1999**, 2305.
[18] J. P. Williams, N. M. Nibbering, B. N. Green, V. J. Patel, J. H. Scrivens. Collision-induced fragmentation pathways including odd-electron ion formation from desorption electrospray ionisation generated protonated and deprotonated drugs derived from tandem accurate mass spectrometry. *J. Mass Spectrom.* **2006**, *41*, 1277.
[19] M. Schäfer, M. Drayß, A. Springer, P. Zacharias, K. Meerholz. Radical cations in electrospray mass spectrometry: formation of open-shell species, examination of the fragmentation behaviour in ESI-MSn

and reaction mechanism studies by detection of transient radical cations. *Eur. J.Org. Chem.* **2007**, *31*, 5162.
[20] X.-S. Miao, R. E. March, C. D. Metcalfe. A tandem mass spectrometric study of the *N*-oxides, quinoline *N*-oxide, carbadox, and olaquindox, carried out at high mass accuracy using electrospray ionization. *Int. J. Mass Spectrom.* **2003**, *230*, 123.
[21] R. Vessechi, S. E. Galembeck, N. P. Lopes, P. G. B. D. Nascimento, A. E. M. Crotti. Aplicação da química quântica computacional no estudo de processos químicos envolvidos em espectrometria de massas. *Quim Nova.* **2008**, *31*, 840.
[22] K. H. M. Cardozo, R. Vessecchi, V. M. Carvalho, E. Pinto, P. J. Gates, P. Colepicolo, S. E. Galembeck, N. P. Lopes. A theoretical and mass spectrometry study of the fragmentation of mycosporine-like amino acids. *Int. J. Mass Spectrom.* **2008**, *273*, 11.
[23] A. E. M. Crotti, E. S. Bronze-Uhle, P. G. B. D. Nascimento, P. M. Donate, S. E. Galembeck, R. Vessecchi, N. P. Lopes. Gas-phase fragmentation of γ-lactone derivatives by electrospray ionization tandem mass spectrometry. *J. Mass Spectrom.* **2009**, *44*, 1733.
[24] W. Yang, W. J. Mortier. The use of global and local molecular parameters for the analysis of the gas-phase basicity of amines. *J. Am. Chem. Soc.* **1986**, *108*, 5708.
[25] R. S. Mulliken. Electronic population analysis on LCAO-MO molecular wave functions. I. *J. Chem. Phys.* **1955**, *23*, 1833.
[26] A. E. Reed, L. A. Curtiss, F. Weinhold. Intermolecular interactions from a natural bond orbital, donor-acceptor viewpoint. *Chem. Rev.* **1988**, *88*, 899.
[27] R. R. Contreras, P. Fuentealba, M. Galván, P. Pérez. A direct evaluation of regional Fukui functions in molecules. *Chem. Phys. Lett.* **1999**, *304*, 405.
[28] C. Denekamp, E. Tenetov, Y. Horev. Homolytic cleavages in pyridinium ions, an excited state process. *J. Am. Soc. Mass Spectrom.* **2003**, *14*, 790.
[29] H. T. Le, P. Gerbaux, R. Flammang, M. T. Nguyen. Collisional activation of protonated halogeno-pyridines: different behaviour of target gases. *Chem. Phys. Lett.* **2000**, *323*, 71.
[30] A. Albini, M. Alpegiani. The photochemistry of the *N*-oxide function. *Chem. Rev.* **1984**, *84*, 43.
[31] P. Ballesteros, R. M. Claramunt, T. Cañada, C. Foces-Foces, F. Hernández-Cano, J. Elguero, A. Fruchier. A ^{1}H and ^{13}C nuclear magnetic resonance and X-ray diffusion study of the tautomerism of 2-hydroxy- and 2,3-dihydroxy-pyridine *N*-oxides. X-ray molecular structure of 2-hydroxypyridine *N*-oxide. *J. Chem. Soc. Perkin Trans. 2.* **1990**, *7*, 1215.